ACS Combinatorial Science

Research Article

pubs.acs.org/acscombsci

Colorimetric Screening for High-Throughput Discovery of Light Absorbers

Slobodan Mitrovic,* Edwin Soedarmadji, Paul F. Newhouse, Santosh K. Suram, Joel A. Haber, Jian Jin,† and John M. Gregoire*

Joint Center for Artificial Photosynthesis, California Institute of Technology, Pasadena, California 91125, United States

†Engineering Division, Lawrence Berkeley National Laboratory, Berkeley, California 94720, United States

Supporting Information

ABSTRACT: High-throughput screening is a powerful approach for identifying new functional materials in unexplored material spaces. With library synthesis capable of producing 10^5 to 10^6 samples per day, methods for material screening at rates greater than 1 Hz must be developed. For the discovery of new solar light absorbers, this throughput cannot be attained using standard instrumentation. Screening certain properties, such as the bandgap, are of interest only for phase pure materials, which comprise a small fraction of the samples in a typical solid-state material library. We demonstrate the utility of colorimetric screening based on processing photoscanned images of combinatorial libraries to quickly identify distinct phase regions, isolate samples with desired bandgap, and qualitatively identify samples that are suitable for complementary measurements. Using multiple quaternary oxide libraries containing thousands of materials, we compare colorimetric screening and UV−vis spectroscopy results, demonstrating successful identification of compounds with bandgap suitable for solar applications.

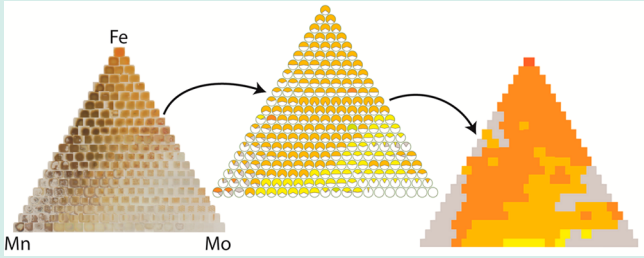

KEYWORDS: *high-throughput, colorimetry, light absorbers, solar fuels*

INTRODUCTION

Although accelerated discovery of solid-state materials for advanced technologies benefits tremendously from high-throughput combinatorial synthesis,[1,2] the throughput of screening techniques for relevant physical properties is not generally matched to the synthesis throughput. In our search for new catalysts and light absorbers for solar fuel technologies,[3,4] we use high-speed inkjet printers capable of daily outputs of hundreds of thousands of samples.[5] Matching this production rate requires material screening faster than one sample per second, which cannot generally be performed using serial measurements. It is therefore desirable to have appropriate, less accurate, lower quality methods that can evaluate samples in parallel and identify select samples for high-quality experiments, and such down-selection experiments can employ one or more of the following strategies: (i) detection of samples or broad composition regions displaying a desired metric; (ii) identification of samples not suitable for slower, high-quality serial measurements; (iii) determination of phases, i.e., regions with similar properties that may contain a unique phase or compound. In this article, we present a protocol developed primarily as a prescreening tool for the acceleration of high-throughput ultraviolet−visible (UV−vis) spectroscopy, which we use to evaluate the light absorption and bandgap of semiconductors. We capture images of combinatorial libraries using a commercial photoscanner (EPSON Perfection V600) and then analyze the images with a custom image-processing algorithm described herein. Individual material samples (the Spots) in the library are analyzed for color within the hue−saturation−brightness color space.

Even though there is a direct relationship between color and bandgap in intrinsic semiconducting materials, there are many, often prevailing, causes for color in solids and from solid surfaces.[6] Wide bandgap semiconductors often owe their color to transition metal impurities or to charge transfer between different oxidation states in multivalent transition metal compounds. A high-throughput technique that down-selects samples for further study can be very useful even with a moderate false positive detection rate, so the perceived color can still be used as a metric for identification of desired bandgaps in material libraries. To identify samples that are not suitable for UV−vis spectrometry, we note that the spectrometry data is readily interpreted only for phase-pure materials.[7,8] The presence of multiple colors within one Spot is a strong indication of phase segregation, and exclusion of such samples enhances efficiency of high-throughput spectrometry experiments.

Received: October 2, 2014
Revised: December 9, 2014
Published: December 30, 2014

DOI: 10.1021/co500151u
ACS Comb. Sci. 2015, 17, 176−181

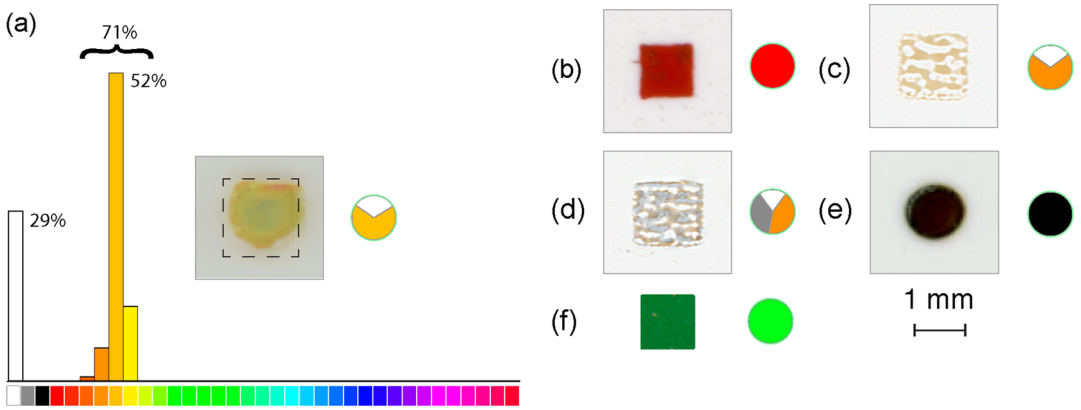

Figure 1. Examples of various Spots from photoscanned combinatorial libraries and the results of the colorimetric scan in the form of a pie chart. The chart accounts for all the pixels within the material Spot and shows the percentage of white (W), gray (G), black (B), or a hue value categorized into 32 bins. For a, the analysis of the spot is shown as both a histogram and pie chart, and the pie chart representation is shown for Spots b–f.

To segment the composition library into composition regions of similar optical properties, we identify and group materials by their dominant color, often reducing a large composition space into several unique regions, from which representative samples can be chosen for further study. We find these regions to match those apparent in Tauc plot data from the high-quality serial scanning. Segmentation of large composition spaces is an indication of similarity in material phase or properties and is therefore a potentially useful prescreen for many other techniques, in particular, characterization techniques such as X-ray photoelectron spectroscopy, X-ray diffraction, or Raman spectroscopy.

RESULTS AND DISCUSSION

Colorimetric Screening Algorithm. Commercial photo scanners are designed to reproduce the color of an object as perceived by an average human in daylight, which involves the reflection and transmission of visible light by the scanned medium. The scanner uses a broadband illumination source and imaging optics that include mirrors to create separate beam paths containing a red, green, or blue filter and an 8-bit high-density monochrome charge-coupled device (CCD) detector. The intensities from the three channels are then interpreted and stored as a 24-bit color gamut image in the red–green–blue (RGB) color space. However, color is more intuitively perceived and more directly attributable to reflective/absorptive properties if analyzed in the hue–saturation–brightness (HSB) color space. Hue represents the chromatic aspect of color. Saturation and brightness represent the gamut of a given hue in the direction of the loss of chromaticity toward gray and toward black, respectively (see Figure S2a in Supporting Information). Colorimetric analysis of materials is often performed in the Commission Internationale de l'éclairage La*b* space (CIELAB), which is designed to accurately approximate human vision. It has been applied to the optical analysis of combinatorial libraries of oxide thin films,[9] to the combinatorial discovery of fluorescent materials,[10] and for following nitrogen content in combinatorial libraries of nitride thin films.[11] Both CIELAB and HSB originate from the same Munsell color system and can be related through a simple mathematical transformation. We choose HSB in the present work because, unlike CIELAB, a single parameter (hue) sufficiently describes the entire chromatic aspect and the compositional variation of this parameter segments the combinatorial compositional space.

We apply colorimetric screening to discrete composition libraries prepared by an inkjet-printing technique, as described previously.[5] The inkjet-printed Spots are about 1 mm^2 in size, and several example images are shown in Figure 1. The result of the colorimetric algorithm for a given Spot is a pie chart that represents the color distribution of the collection of pixels within the corresponding region of the library image. The pie chart shows the fractions of pixels that fall under one of 35 different values (Figure 1a). Thirty-two of these values represent the detected hue. Hue is typically represented using a cyclical scale with values from 0 to 360°. We find that the results are most easily interpreted if this gamut is binned into 32 values. More than 32 values would give distinction to essentially the same reflective/transmissive properties, and fewer than 32 values removes some ability of the technique to distinguish different semiconductor materials. The other three values found in the pie chart give information on pixels with zero chromaticity and are labeled as white (W), gray (G), and black (B). If achromaticity is the result of low saturation, then the pixels are binned as G, and if it is due to low brightness, then they are labeled B. W designates pixels with HSB values matching those of the (optically transparent) substrate, which is achromatic. The saturation and brightness thresholds for G and B are adjustable parameters. We find that B smaller than 20% and S less than 10% define well the pixels with undefined chromaticity (Figure S2b). Physically, this lack of chromaticity is the result of equal light intensities from each one of the three CCD recordings inside the scanner. In such cases, the achromatic regions of an image have large pixel-to-pixel variation of hue assignment. Figure 1 shows several representative examples of Spot images and their colorimetric analysis results.

The 32 hue values and 3 achromatic values are shown in Figure 1a. This figure shows a Spot image and the colorimetric algorithm output in the form of a histogram, from which the pie chart representation is derived. The inset shows the corresponding Spot and the region of 2601 pixels that were used in the colorimetric algorithm. Twenty nine percent of the pixels have the same value as that of the substrate (W) due to incomplete coverage of the sample in the 1 mm^2 analysis region. Since all of the detected hues are a part of the same peak in the hue histogram, a single hue value is assigned to this

DOI: 10.1021/co500151u
ACS Comb. Sci. 2015, 17, 176–181

Spot, equal to the hue of the maximum in the histogram. Other Spots in Figure 1 show a range of illustrative examples: (b) a square Spot with a uniform hue value; (c) a square Spot with a single hue, but discontinuous on the substrate, and therefore having W pixels; (d) a square sample spot with discontinuities and two segregated phases, one with a well-defined hue and another interpreted as gray (G) due to low saturation value; (e) a highly absorbing Spot with low brightness and thus poorly defined hue, which is interpreted as black (B); and (f) the cropped region of a continuous composition spread made by physical vapor deposition (PVD), representing a sample with a single hue value. There is no surrounding background in the cropped image from the continuous PVD library. The scale bar in the lower right corner pertains to all photoscanned images.

The histogram data (Figure 1a) can be presented in various ways depending on the purpose of the analysis. In Figure 2b–d, we show three types of colorimetric plots compared against the photoscanned images of Spots assembled into ternary compositional space in Figure 2a. Figure 2b contains the pie chart representation of the color screen analysis. A more practical representation of this data is shown in Figure 2c, where only the dominant hue is displayed for each composition; all other hues are aggregated and displayed as white. In this data reduction step, all zero-chromaticity pixels (G + W + B) are presented as gray. This representation makes it easier to spot color trends, but, at the same time, it gives insight into homogeneity of the material. Finally, all information but the dominant hue can be ignored, as in Figure 2d, in order to clearly identify composition regions of interest for sample down-selection algorithms.

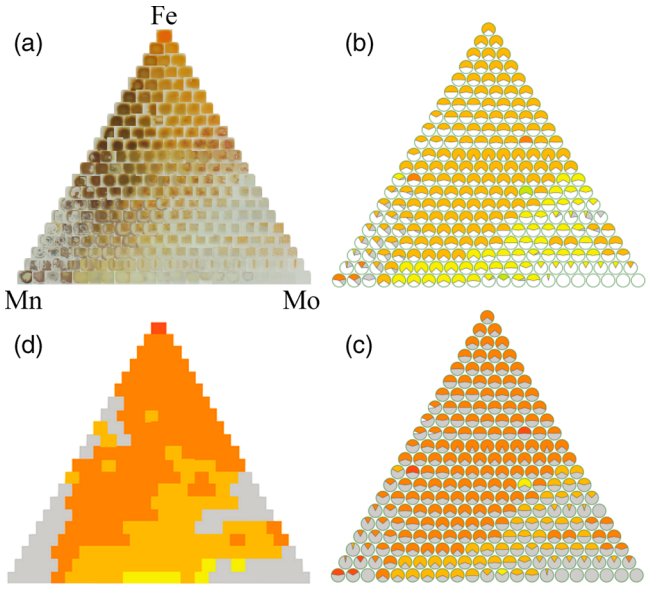

Figure 2. Representations of colorimetric screening data. (a) The assembly of photoscanned images of Spots into a ternary composition space of oxides. The nominal composition step is 5 atomic percent. (b) The representation showing multiple major hues, G, B, and W pixels. (c) Representation showing only one major hue and grouping all nonchromatic pixels together as G. W groups all other, nondominant hues. (d) Representation in which only the dominant component (whether hue or G or B) is plotted.

Screening the Suitability for Additional Experiments. Samples can be flagged as suitable or unsuitable for a particular measurement method based on the colorimetric screen. Figure 1d shows a sample that has two materials with different absorption properties, which makes the sample unsuitable for optical measurements in which the response will be convoluted, such as bandgap analysis via UV–vis spectroscopy and spectral incident photon conversion efficiency (IPCE) measurements. Samples that have uniform color, but are not uniformly distributed, such the sample in Figure 1c, are not good candidates for quantitative optical absorptivity measurements, but a bandgap measurement may still be performed.

While the primary purpose of this report is to demonstrate the utility of the color screening technique for assessing material properties and trends, we also note that Figure 2 shows an example identification of a synthesis error. In the Mn-rich region, Figure 2a shows images of Spots with very low coverage of material due to a synthesis issue. In the color screen analysis, these spots have no dominant hue and are marked as G, making them unsuitable for further optical characterization.

Identification of Promising Light Absorbers. Here, we described the application of the colorimetric screen as a fast, parallelized prescreening for UV–vis spectroscopy. In particular, colorimetric screening can be used as both a negative and positive metric down-selection tool for solar fuels applications. In order to obtain high solar-to-hydrogen conversion efficiency, light absorbers with the bandgap of 1.6–1.8 eV are highly desirable.[12] Naturally, this bandgap energy range falls conveniently into the visible spectrum and can be correlated to appearance of red–orange hues. As a negative metric, all gray and transparent samples are likely to have a wide bandgap with no significant absorption in the visible range. Black Spots can similarly be considered to have a narrow bandgap, in the infrared region. Since false negatives are undesirable in prescreening down-selection, we need to experimentally observe if there are instances where these assumptions do not hold.

Figure 3a shows a photoscanned image of a material library of Bi–Mn–V–Ce oxides. The Spots are cropped and assembled into ternary compositional spaces in Figure 3b. The complete quaternary data sets can be found in Supporting Information. Figure 3c,d shows the corresponding colorimetric screening results and the extrapolated direct allowed bandgap from Tauc plot analysis of transmission-based absorption measurement. The color scale in Figure 3d is chosen so that the bandgaps of interest appear as red or orange.

Many composition trends in Figure 3d were well-characterized by the color screen result of Figure 3c. In particular, the only composition region to exhibit a deep orange dominant hue is near the midpoint of the Mn–V binary line. In this region, Figure 3d shows that the identified bandgaps are in the 1.7–1.9 eV range, and these promising light absorber compositions merit further investigation.

Very few metal oxides have a direct bandgap in the 1.6–1.8 eV range. To date, we have analyzed 38 pseudoquaternary libraries containing a total of 21 unique elements and a total of almost 70 000 different Spots. Each of these spots was characterized using both the color screen and UV–vis spectrometry, and every measured bandgap in the 1.6–1.8 eV range was correctly identified by the dominant hue calculation, demonstrating the absence of false negatives in this high-throughput down-selection method.

Gray Spots (indicative of bandgap in the ultraviolet) and black Spots (indicative of bandgap in the near-infrared) can be used as a negative metric. We expect, however, that the two will not serve as good negative screens in the following situations:

DOI: 10.1021/co500151u
ACS Comb. Sci. 2015, 17, 176–181

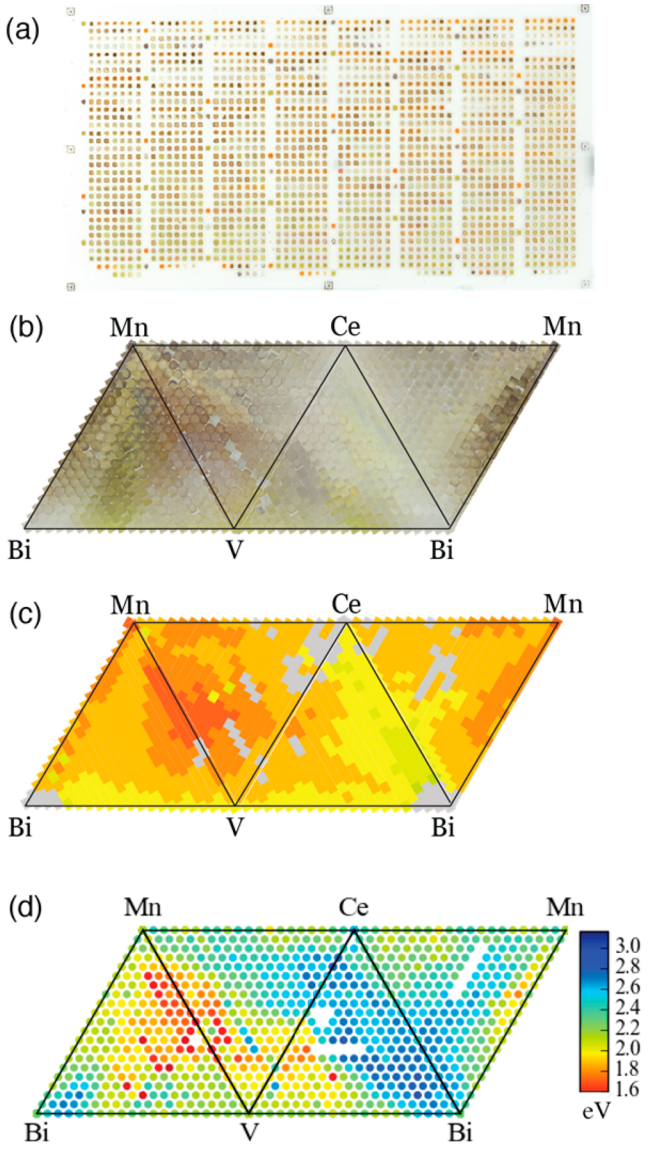

Figure 3. Results of the colorimetric analysis of a quaternary oxide library compared to UV−vis spectroscopy results. (a) A photoscanned image of a library plate containing bismuth, manganese, vanadium, and cerium oxides. (b) Cropped Spots assembled into ternary spaces. (c) The dominant hue identified by the colorimetric analysis. (d) The plot of the estimated direct allowed bandgap from Tauc plot analysis of UV−vis data.

(1) Samples can appear black even when they have a finite absorption anywhere in the visible range, if there is sufficient thickness for all light to be absorbed; (2) samples can appear transparent (hence, gray), even if they have finite absorption in the visible range, if they are thin enough. In our inkjet-printed libraries the Spots are typically 200−600 nm thick, and we find that at that thickness there is an excellent correlation between wide bandgap materials and their gray appearance. On the other hand, thin materials rarely appear black, partly because transition metal oxides typically have bandgaps much larger than 1 eV.[4]

Identifying Possible Phase Fields. Comparing the UV−vis and colorimetry data in Figure 3 reveals excellent agreement in the composition trends. The composition regions with similar bandgap in the serial UV−vis analysis were identified as having similar color in the parallel screen. By clustering composition samples using the colorimetry data, representative samples can be chosen for UV−vis spectroscopy to provide a high-throughput, yet accurate, representation of the entire system.

A unique cluster from colorimetry screening may correspond to a set of compositions that have crystallized (in whole or in part) into a predominant phase. In Figure 4, we have an

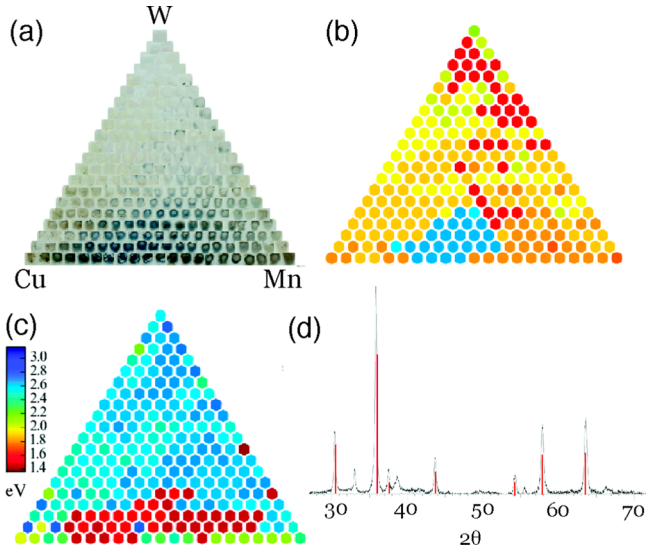

Figure 4. Detecting a material phase using colorimetry. (a) Photoscanned images show a darker, blue-tinted region on the Cu−Mn compositional line. (b) A blue hue phase appears in the colorimetric screen. (c) The plot of the direct allowed bandgap values from automated Tauc plot analysis shows a very low bandgap value of about 1.4 eV for the Mn−Cu line, much smaller than any of the other compounds in the system. (d) XRD confirms that the blue hue region corresponds to a small bandgap material $Cu_{1.5}Mn_{1.5}O_2$.

example of a W−Cu−Mn oxide space (Figure 4a) where colorimetry shows a cluster of a blue hue along the Mn−Cu line. UV−vis data in Figure 4c reveals a much lower bandgap for this region than that from any of the single metal oxides in this ternary space. The measured bandgap is in the near-infrared, so the blue hue is not a direct result of the bandgap of the material, yet this color can be used to distinguish the composition region in which a particular phase dominates the optical properties of the samples. X-ray diffraction identifies the material as $Cu_3Mn_3O_4$, a known light absorber with near-infrared bandgap that has been studied for photocatalytic evolution of hydrogen.[13]

Throughput of Colorimetric Screening. The overall throughput of the colorimetric screening combines the photoscanning and colorimetric algorithm throughputs. Photoscanning is performed over the entire flatbed surface, whose area is 8.47 × 11.67 square inches, on which we place two material libraries. The scan is completed within 160 s, at a resolution of 1200 dpi. Since two library plates contain approximately 1800 samples, the effective throughput with 1 mm^2 area samples is 22.5 samples per second at spatial resolution of 21 μm. With a different arrangement of samples, the maximum throughput of the scanning process can be an order of magnitude higher, as the sample spots would occupy less than 6% of the surface of the flatbed.

Each scanner image is processed with custom image analysis routines to extract images of individual samples and apply the

DOI: 10.1021/co500151u
ACS Comb. Sci. 2015, 17, 176−181

colorimetric algorithm on the individual images. The entire process can be performed at a rate of about 10 samples per second on a modern personal computer. Further parallelization of the process could achieve much faster rates.

Validation of the Screening Method for Materials Discovery. Finally, we look at the relevance of the above-described methodology for discovery of practical functional materials. In the high-throughput discovery approach, thin films are made by combinatorial inkjet printing or physical vapor deposition, and the above methodology is developed for screening of such systems. To validate the results of the combinatorial experiments, we perform a bulk powder synthesis of a composition from the combinatorial library and compare the optical properties measured by colorimetry and spectroscopy. The most promising light absorber compositions identified in Figures 2−4 surround the $Mn_{0.5}V_{0.5}O_x$ sample of Figure 3. To synthesize a bulk powder, equal quantities of 0.25 M $MnCl_2$ containing 10 vol % diethylene glycol and 0.25 M $VOSO_4$ containing 20 vol % diethylene glycol (all from Sigma-Aldrich) were combined and thoroughly stirred to ensure complete mixing. This solution was condensed in a forced-air oven at 72 °C for 1 h and subsequently placed into an alumina crucible and heated under 100 sccm of 20% O_2 with Ar balance at 600 °C for 1 h. The ramp rate was 10 °C/min. The sample of the resulting metal oxide powder was dispersed onto a glass slide for colorimetry and spectroscopy characterization. Figure 5 shows an image of the powder using the photoscanner, where

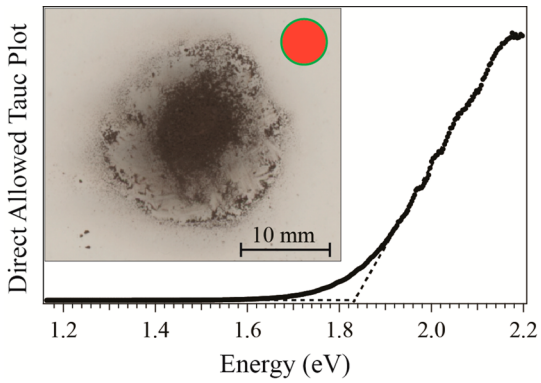

Figure 5. Characterization of a $Mn_{0.5}V_{0.5}O_x$ bulk powder synthesized to reproduce the combinatorial identification of a composition region with 1.7−1.9 eV bandgap, as shown in Figure 3. The inset shows a photoscan of the powder with the primary hue of the optically opaque region displayed in the corner of the image. The Tauc plot calculated from a diffuse reflectance measurement of the bulk powder is shown along with the extrapolation (dotted line), indicating a bandgap energy near 1.8 eV (dotted line), in excellent agreement with the results from the combinatorial thin-film library.

the thickness of the powder produces an optically opaque region in the center of the image. Color analysis of this region shows that the average brightness varies from 18−26% and that saturation in all pixels is above 13%, both within our typical limits for the automated colorimetric screening algorithm. The hue values range between 12 and 27°, which falls within hue bin 2 shown in Figure 1. As shown in Figure 3, the composition region in the combinatorial library exhibits hue bins 2−4, demonstrating excellent agreement between the bulk powder and thin film library.

Spectrometry characterization of the $Mn_{0.5}V_{0.5}O_x$ bulk sample was done using the standard method of diffuse reflectance of optically thick powders. A broadband light source illuminates the powder, with light collected by an integrating sphere with a blocked specular reflectance port. These measurements are used to determine the spectral reflectance, which is then used in Tauc plot analysis. The direct allowed Tauc plot in Figure 5 confirms that the powder has a bandgap in the desired range, approximately 1.8 eV, which is in excellent agreement with the range of bandgap values identified in the combinatorial library.

CONCLUSIONS

We have demonstrated that colorimetric analysis based on HSB color space can be used as a simple but effective tool in the search for light absorbers for solar fuel applications. Colorimetry can be used to identify materials with a desirable bandgap in the visible range or to determine whether the bandgap of a semiconductor falls into near-infrared or ultraviolet. The method can therefore enable quick down-selection for UV−vis spectroscopy in high-throughput discovery. At the same time, the information is helpful in determining homogeneity of samples and for general phase-space segmentation in combinatorial research.

EXPERIMENTAL PROCEDURES

Photoscanning. We use an EPSON Perfection V600 flatbed scanner in the reflection configuration. Transparent glass plates with combinatorial libraries are placed facing up, away from the flatbed surface and touching the white reflective backing of the scanner lid. In this way, the samples are in contact with the reflective material, but they are about 2 mm out of the focal plane. This configuration was necessary to mitigate shadowing of the translucent samples. Libraries on nontransparent substrates, such as silicon wafers and metal plates, are placed on the scanner face down, with samples facing the flatbed surface. The images are acquired at 1200 dpi resolution (21.2 μm physical resolution) and 24-bit color depth (from three monochrome sensors, each with 8-bit resolution) and saved into an uncompressed tagged image file format (TIFF).

UV−Vis Spectroscopy. The bandgap data is derived from transmission spectra collected by a custom high-speed UV−vis scanner. The details of the instrument and data processing algorithms will be presented in a separate publication. Briefly, a transmission spectrum for a given sample is normalized by a reference spectrum, providing the spectral transmission. The absorption coefficient of the sample and the transmission are related according to the Beer−Lambert equation with $\alpha \propto \ln(T)$. In the Tauc formalism, the absorption of a direct bandgap semiconductor follows $\alpha h\nu \propto (h\nu - E_g)^2$, where h is Planck's constant, ν is the frequency of light, and E_g is the bandgap of the electronically allowed transition. Using the Tauc relationship, E_g is typically measured as the intercept between tangents corresponding to absorption onset and background regions of the spectrum. An automated algorithm for identifying the intercept for each spectrum produces an estimation of the direct bandgap for each Spot. For the purposes of this article, we are not concerned with identifying an indirect and/or forbidden electronic gap with energy lower than that of the observed optical gap. For a given composition space, the interpretation of UV−vis transmission spectra produces a compositional map of the apparent optical gap energy, which serves as a useful comparison to the composi-

DOI: 10.1021/co500151u
ACS Comb. Sci. 2015, 17, 176−181

tional trends produced by the high-throughput colorimetry experiment.

■ ASSOCIATED CONTENT

Supporting Information

Photoscanning and colorimetric algorithm. Complete results from a quaternary library of Bi−Mn−V−Ce oxides. Tauc plot for $Cu_{1.5}Mn_{1.5}O_2$. This material is available free of charge via the Internet at http://pubs.acs.org.

■ AUTHOR INFORMATION

Corresponding Authors

*(S.M.) E-mail: mitrovic@caltech.edu; Tel.: 626-395-2613; Fax: 626-395-1577.

*(J.M.G.) E-mail: gregoire@caltech.edu; Tel.: 626-395-2613; Fax: 626-395-1577.

Author Contributions

The manuscript was written through contributions of all authors. All authors have given approval to the final version of the manuscript.

Notes

The authors declare no competing financial interest.

■ ACKNOWLEDGMENTS

The authors thank Ryan J. R. Jones for assistance with the experiments. This manuscript is based upon work performed by the Joint Center for Artificial Photosynthesis, a DOE Energy Innovation Hub, supported through the Office of Science of the U.S. Department of Energy (award no. DE-SC0004993).

■ REFERENCES

(1) Green, M. L.; Takeuchi, I.; Hattrick-Simpers, J. R. *J. Appl. Phys.* **2013**, *113*, 231101.

(2) Gregoire, J. M.; Xiang, C.; Mitrovic, S.; Liu, X.; Marcin, M.; Cornell, E. W.; Fan, J.; Jin, J. *J. Electrochem. Soc.* **2013**, *160*, F337−F342.

(3) Walter, M. G.; Warren, E. L.; McKone, J. R.; Boettcher, S. W.; Mi, Q. X.; Santori, E. A.; Lewis, N. S. *Chem. Rev.* **2010**, *110*, 6446−6473.

(4) Cook, T. R.; Dogutan, D. K.; Reece, S. Y.; Surendranath, Y.; Teets, T. S.; Nocera, D. G. *Chem. Rev.* **2010**, *110*, 6474−6502.

(5) Liu, X.; Shen, Y.; Yang, R. T.; Zou, S. H.; Ji, X. L.; Shi, L.; Zhang, Y. C.; Liu, D. Y.; Xiao, L. P.; Zheng, X. M.; Li, S.; Fan, J.; Stucky, G. D. *Nano Lett.* **2012**, *12*, 5733−5739.

(6) Nassau, K. *The Physics and Chemistry of Color*, 2nd ed.; John Wiley & Sons, Inc.: New York, 2001.

(7) Tauc, J. *Mater. Res. Bull.* **1968**, *3*, 37−46.

(8) *Amorphous and Liquid Semiconductors*; Tauc, J., Ed.; Plenum Press: London, 1974; Chapter 4.

(9) Perkins, J. D.; Teplin, C. W.; van Hest, M. F. A. M.; Alleman, J. L.; Li, X.; Dabney, M. S.; Keyes, B. M.; Gedvilas, L. M.; Ginley, D. S.; Lin, Y.; Lu, Y. *Appl. Surf. Sci.* **2004**, *223*, 124−132.

(10) Wang, J.; Yoo, Y.; Gao, C.; Takeuchi, I.; Sun, X.; Chang, H.; Xiang, X. D.; Schultz, P. G. *Science* **1998**, *279*, 1712.

(11) Niyomsoan, S.; Grant, W.; Olson, D. L.; Mishra, B. V. *Thin Solid Films* **2002**, *415*, 187−194.

(12) Hu, S.; Xiang, C.; Haussener, S.; Berger, A. D.; Lewis, N. S. *Energy Environ. Sci.* **2013**, *6*, 2984−2993.

(13) Bessekhouad, Y.; Trari, M.; Doumerc, J. P. *Int. J. Hydrogen Energy* **2003**, *28*, 43−48.

DOI: 10.1021/co500151u
ACS Comb. Sci. 2015, 17, 176−181